JTTEE5 16:661–668
DOI: 10.1007/s11666-007-9086-8
1059-9630/$19.00 © ASM International



# Investigation of Al-$Al_2O_3$ Cold Spray Coating Formation and Properties

*Eric Irissou, Jean-Gabriel Legoux, Bernard Arsenault, and Christian Moreau*

*(Submitted March 8, 2007; in revised form June 29, 2007)*

**Coating build-up mechanisms and properties of cold-sprayed aluminum-alumina cermets were investigated using two spherical aluminum powders having average diameters of 36 and 81 μm. Those powders were blended with alumina at several concentrations. Coatings were produced using a commercial low-pressure cold spray system. Powders and coatings were characterized by electronic microscopy and microhardness measurements. In-flight particle velocities were monitored for all powders. The deposition efficiency was measured for all experimental conditions. Coating performance and properties were investigated by performing bond strength test, abrasion test, and corrosion tests, namely, salt spray and alternated immersion in saltwater tests. These coating properties were correlated to the alumina fraction either in the starting powder or in the coating.**

**Keywords** abrasion resistance, corrosion protection, gas dynamic spray, low-pressure cold spray, metal-ceramic mixture

## 1. Introduction

The cold gas dynamic spray technique (CGDS), or cold spray, consists in surface coating with high-velocity particles at temperature significantly lower than the melting temperature of deposited materials. The idea of using a compressed gas jet to accelerate metal particles to supersonic velocity in order to produce a coating by impact of the solid particles onto a substrate was patented as early as 1903 (Ref 1) and 1963 (Ref 2). However, successful development of this technique and fabrication of commercial systems emerged only several decades later (Ref 3-5). Nowadays, there exist two categories of such systems, namely the high- and the low-pressure guns working at typical stagnation gas pressure ranges of 2-5 MPa (Ref 6) and 0.3-1 MPa (Ref 5), respectively.

High-pressure systems allow achieving a higher particle velocity as compare to low-pressure systems, which in turn provide higher deposition efficiency and broader range of eligible materials. The major drawback of these systems is high operation costs as they use high-pressure gas ($N_2$ or He) at high-flow rate (120-220 $m^3$/h). In low-pressure systems, metals such as Al, Zn, Cu, Co, and Ni (Ref 4) can be deposited with fairly ''good'' coating properties but with low-deposition efficiency. Niche applications can support this technology because the low-operation costs can overcome the higher powder consumption.

It was shown that the deposition efficiency can be improved by adding hard particles to a metal powder and with proper blend of hard particle the deposition efficiency can reach 20-30%, which is an increase of more than 300% as compare to the deposition efficiency of metals (Ref 4). Also, the use of a ceramic-metal mixture enhanced the coating quality by reducing the porosity (1-7%) of the coating and by increasing the bond strength (40-80 MPa) of the coating to the substrate (Ref 4). Numerous studies were devoted to the fundamentals of the coating build-up process in cold spraying of a mixture of ceramic and ductile powders (Ref 4, 7, 8). However, very limited data about the influence of the inclusion of ceramic particles on cold-sprayed coating performance has been published up to now.

In a previous communication, we have shown that pure Al coatings produced by low-pressure cold spray provide outstanding protection against stress corrosion cracking (Ref 9). Would that property be affected by the inclusion of ceramic particles in the coating powder? This question initially motivated the present study. In this work, the three principle objectives were: (i) investigate the influence of Al particle size and $Al_2O_3$ fraction in Al-$Al_2O_3$ powder mixtures on the coating deposition and properties; (ii) verify if the addition of ceramic particles improves the coating abrasion resistance; (iii) investigate whether or not the inclusion of ceramic particles reduces the corrosion resistance of pure aluminum coatings.

This article is an invited paper selected from presentations at the 2007 International Thermal Spray Conference and has been expanded from the original presentation. It is simultaneously published in *Global Coating Solutions, Proceedings of the 2007 International Thermal Spray Conference*, Beijing, China, May 14-16, 2007, Basil R. Marple, Margaret M. Hyland, Yuk-Chiu Lau, Chang-Jiu Li, Rogerio S. Lima, and Ghislain Montavon, Ed., ASM International, Materials Park, OH, 2007.

**Eric Irissou, Jean-Gabriel Legoux, Bernard Arsenault,** and **Christian Moreau**, National Research Council Canada – Industrial Materials Institute, 75 de Mortagne Blvd., Boucherville, QC, Canada J4B 6Y4. Contact e-mail: Eric.Irissou@cnrc-nrc.gc.ca.

## 2. Experimental Procedure

### 2.1 Materials

Two commercially available Al powders and one alumina powder were used for this study. The first Al powder labeled 54NS was provided by Sulzer Metco and the second Al powder labeled 10576 was obtained from Alfa-Aesar. The $Al_2O_3$ powder, labeled PT105C, was provided by Plasmatec. Al powders were mixed to $Al_2O_3$ at concentrations of 7, 10, 20, 30, 50, and 75% mass fraction.

### 2.2 Coatings

Pure Al powders and Al-$Al_2O_3$ powder mixtures were cold sprayed onto mild steel and Al7075 substrates using a low-pressure cold spray system (SST, Centerline, ON, Canada). For all experiments, the inlet nitrogen gas temperature and pressure were fixed at 500 °C and 0.62 MPa, respectively. The gun was held by a robot at a constant standoff distance of 1 cm and moved across the substrate surface at a transverse speed of 2 mm/s. The powder was fed at 8-12 g/min using an external powder feeder with nitrogen carrier gas at a flow rate of 3 L/min. Prior to deposition, the substrates were either grit blasted using 24 grit alumina or polished at 1200 grits.

### 2.3 Characterization

The volume-weighted powder size distributions were measured using a laser diffraction particle size analyzer (LS320, Beckman Coulter, Miami, FL, USA). Particle velocity measurements were performed using a time-of-flight particle diagnostic system (DPV2000) (Tecnar Automation, St-Bruno, QC, Canada), operated in cold particle mode using a laser diode (7 W, $\lambda = 830$ nm) to illuminate the in-flight particles. Deposition efficiency was determined on 3 mm-thick grit blasted mild steel substrates weighted before and after deposition. Materials characterization was performed by field emission scanning electron microscopy (S4700, Hitachi, Tokyo, Japan) and Vickers hardness measurements. Coating properties were investigated by means of bond strength, abrasion, and corrosion tests. Bond strength measurements were performed according to ASTM C-633-99 standard. About 370-430 μm thick coatings were applied to the top flat surface of 2.54 cm diameter cylinder coupons. Epoxy ESP310 was used to glue the counter block on the coupons. Abrasion tests were performed according to the ASTM G-65-00 procedure D standard with a load of 45 N during 10 min. The thickness of the coatings was in the 550-650 μm range for these abrasion coupons. Two corrosion tests were performed: a salt spray (3.5% NaCl) environment test using the ASTM G 85 standard and an alternated immersion in saltwater test using the ASTM G 44-99 standard. This latter test consists in immersing the samples in a 3.5% NaCl solution for a period of 30 min and then pumping the solution out of the test vessel leaving the sample in this dry environment for another 30 min and then repeating this procedure for a total duration of 1000 h.

## 3. Results and Discussion

### 3.1 Powder Characterization

Figure 1 shows the results of the characterization of the three powders used in this work. The $Al_2O_3$ particles are angular in shape and exhibit high-hardness value of about 2000 $HV_{10}$. The powder size distribution is symmetrical with a mean size and standard deviation of 25.5 and 8.8 μm, respectively. The 54NS Al powder is mostly spherical in shape with small particles agglomerated on the large ones. The hardness value was found to be $25 \pm 3$ $HV_{10}$. The mean particle size and standard deviation are equal to 81.5 and 23.1 μm, respectively, and the distribution is asymmetrical with a non-negligible volume fraction in the 120-180 μm range. Finally, the Al powder from Alfa-Aesar exhibits a very similar particle shape than that of the 54NS with, however, lesser small aggregated particles. The hardness value was found to be similar to the 54NS powder being $26 \pm 2$ $HV_{10}$. As shown in Fig. 1, the Alfa Al powder has a bimodal distribution with two groups of particle about 35 and 80 μm. This latter group represents about 10% of the total volume. The mean particle size and standard deviation are 36.2 and 16.4 μm, respectively. Thereafter, the 54NS powder is labeled the large Al powder and the Alfa-Aesar powder is labeled the small Al powder.

### 3.2 Coating Microstructures

Figure 2 compares typical micrographs obtained for pure Al and Al-$Al_2O_3$ coatings using the two Al powders. Samples were etched in order to reveal the particle boundaries between particles. The coating obtained using the large Al powder (Fig. 2a) exhibits a porous microstructure. This coating exhibited a weak adhesion to the substrate as testified by its delamination from the substrate during metallographic preparation. On the contrary, the coating obtained using the small Al powder (Fig. 2c) shows a very dense microstructure and good adhesion to the substrate. The particles of the large Al powder in the porous regions of the coating in Fig. 2a seem to be less deformed than the particles of the small Al powder coating in Fig. 2c. However, in the dense regions, the smaller particles of the large Al powder were heavily deformed, their flattening ratio being higher than that found in the small Al powder coating.

The most stricking result shown in Fig. 2 is the difference between the pure large Al powder coating (Fig. 2a) and the large Al-$Al_2O_3$ coating (Fig. 2b). Adding only 7 wt.% of $Al_2O_3$ to the large Al powder resulted in the build-up of a dense coating with strong adhesion to the substrate. The high level of deformation of the Al particles is also remarkable. For the small Al powder, adding alumina resulted in a coating with a microstructure similar to that obtained with the large Al-$Al_2O_3$ powder (Fig. 2d). All coatings presented in Fig. 2 were deposited onto a polished Al7075 substrate. It can be seen that none of the pure Al coatings have roughen the substrate surface during deposition while for the two Al-$Al_2O_3$ coatings significant roughening of the substrate surface was

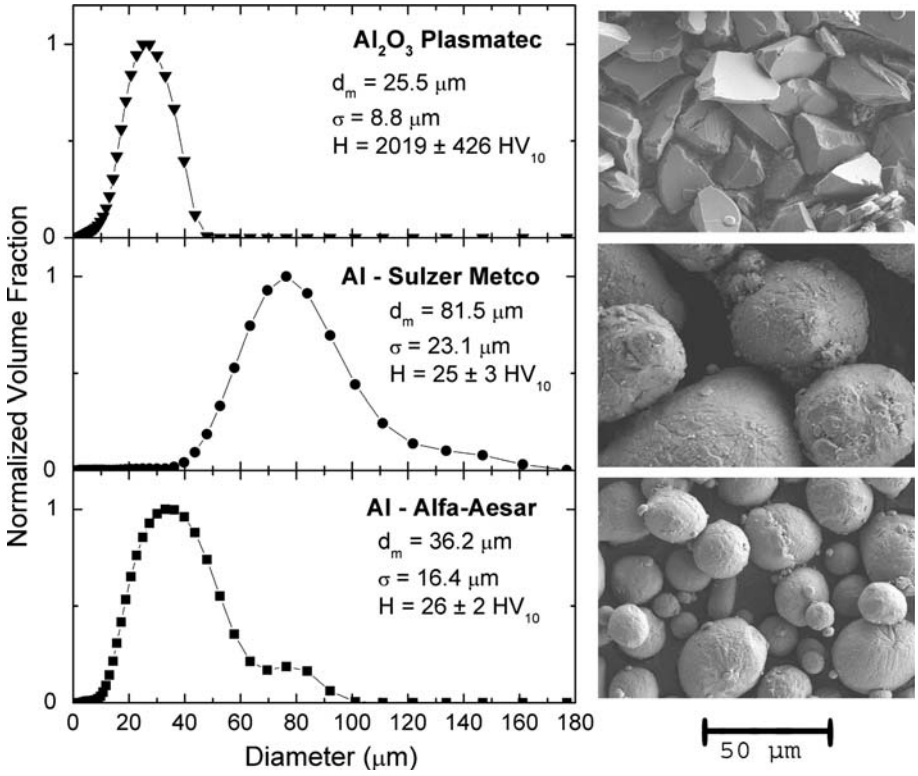


**Fig. 1** Powder size distributions and SEM micrographs for the 10576 Al powder from Alfa-Aesar, the 54NS Al powder from Sulzer Metco and the PT105C $Al_2O_3$ powder from Plasmatec. Mean particle sizes with their standard deviations are given along with Vicker's hardness values

observed indicating that a significant erosion of the surface was caused by the hard particles. This concomitant erosion has been reported to enable the adhesion at lower gun pressure or particle velocities (Ref 7, 10).

### 3.3 Deposition Efficiency

The deposition efficiency of the two mixture types is plotted in Fig. 3 as a function of the ceramic mass fraction of the starting powder. Square symbols represent the Al-$Al_2O_3$ deposition efficiency, calculated from the mass increase of the substrate after coating, knowing the feed rate and duration of the coating process. Circle symbols represent the Al deposition efficiency calculated from the mass increase of the Al content alone into the coating with respect to the mass fraction of the sprayed starting powder. These last results are based on the known Al to $Al_2O_3$ ratios in the coating and powder mixture. It can be seen that the deposition efficiency of both Al types increases significantly with the addition of $Al_2O_3$ particles. Optimum deposition efficiency was found to be about 30 wt.% of $Al_2O_3$ in the starting powder. The deposition efficiency increases from 1.25 to 5.9% and from 8.3 to 11.8% when the $Al_2O_3$ concentration is increasing from 0 to 30 wt.% for the large and the small Al powders, respectively. Similar trends and optimum ceramic ratio were also observed by Shkodkin et al. (Ref 4).

Figure 4 compares the $Al_2O_3$ mass fraction entrapped into the coating, as measured by SEM image analysis, with the $Al_2O_3$ mass fraction in the starting powder. One can see that, for above 10 wt.% $Al_2O_3$ in the starting powder, the increase of $Al_2O_3$ does not lead to a corresponding linear increase of $Al_2O_3$ into the coatings. According to this behavior, the maximum $Al_2O_3$ concentration incorporated into the coatings is somewhere about 25 wt.% for both Al-$Al_2O_3$ powder mixtures. The powder mixture with the small Al results in a higher $Al_2O_3$ concentration into the coating as compared to the powder mixture using the 54NS.

This limitation results from the fact that $Al_2O_3$ cannot be deposited on $Al_2O_3$. Our experiments showed nearly zero deposition efficiency for pure $Al_2O_3$ powder deposition (Fig. 3). In the range of velocity measured, ceramic particles can adhere only on ductile surface, thus only a monolayer of $Al_2O_3$ could be deposited on Al independently of the number of passes. Consequently, the more $Al_2O_3$ is included in the starting powder, the higher is the probability that an $Al_2O_3$ particle hit another $Al_2O_3$ particle. These particles simply rebound and fragment the impacted particles. Indeed, higher is the concentration of $Al_2O_3$ in the starting powder, higher is the amount of fragmented $Al_2O_3$ particles observed by SEM (not shown).

### 3.4 In-Flight Velocity Measurements

The in-flight particle velocities as a function of spray conditions were measured for the three powders. All three

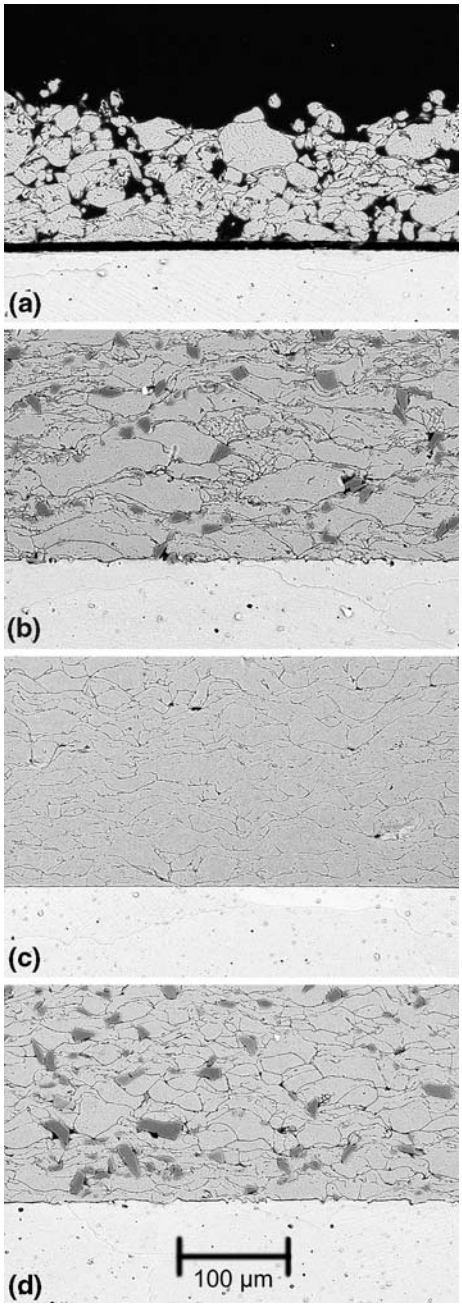


**Fig. 2** Back-scattered electron micrographs of etched cold spray coatings cross section obtained with (a) the large Al powder (54NS), (b) the large Al (54NS) + 7 wt.% $Al_2O_3$ powder mixture, (c) the small Al (Alfa-Aesar) powder, and (d) the small (Alfa-Aesar) Al + 10 wt.% $Al_2O_3$ powder mixture

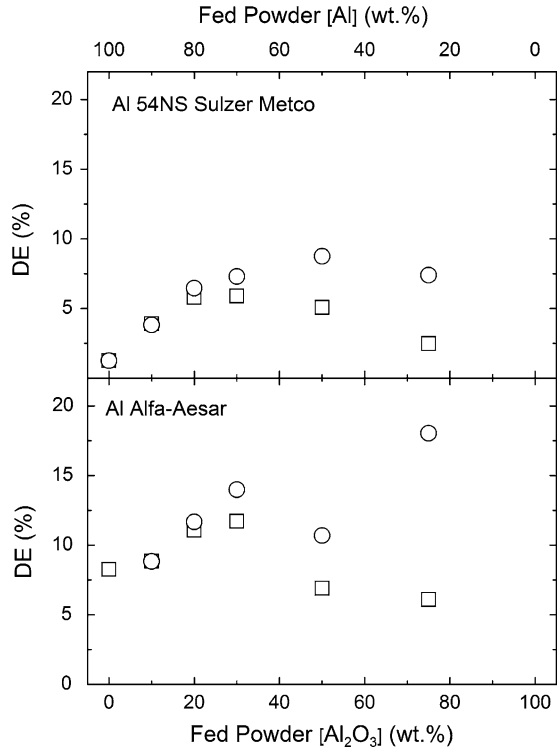


**Fig. 3** Deposition efficiencies of (□) the blended Al-$Al_2O_3$ powder and (○) the Al content of the powder for the large (54NS Sulzer Metco) and the small (Alfa-Aesar) Al powders blended with $Al_2O_3$

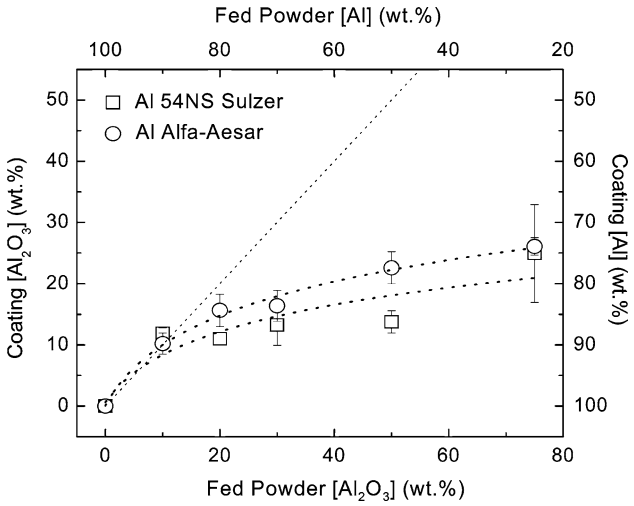


**Fig. 4** $Al_2O_3$ concentration measured in coatings as a function of the starting powder $Al_2O_3$ concentration. The line has a slope of 1

velocity distributions are symmetrical with a nearly Gaussian shape. Mean velocities for the large Al (54NS) and for the small Al (Alfa) powders were measured to be equal to 448 and 584 m/s (Table 1), respectively. As the mean particle sizes of the large and small Al powders are 81 and 36 μm, respectively, these results are close to obey the fluid dynamics law $v \propto 1\sqrt{d \cdot \rho}$, where the mean velocity $v$ is inversely proportional to the square root of particle diameter $d$ and material density ρ. For $Al_2O_3$, the particles mean velocity was found to be 580 m/s. The $Al_2O_3$-to- small Al density ratio and mean particle size ratio are equal to 1.37 and 0.7, respectively. Consequently, the rather small difference in velocities found between the

$Al_2O_3$ and small Al particles are in agreement with the velocity relation with particle size and density.

The critical velocity at which Al particles start to stick to a smooth substrate is reported to be about 650-670 m/s for pure Al (Ref 11, 12). Also, a theoretical model predicted a critical velocity ranging between 620 and 670 m/s for 25 μm Al particles on an Al substrate, which was related to the presence of an adiabatic shear instability (Ref 13).

Figure 5 shows the cumulative volume fraction against velocity curves for (a) the large and for (b) the small Al powders. Also, on these graphs, the deposition efficiency, which is 1 minus the cumulative volume fraction, is scaled on the right-end side. According to the deposition efficiency measured for both powders, it is possible, from this graph, to determine what the critical velocities are. The critical velocities were found to be about 680 m/s for both powders. This value is slightly higher than the upper range of reported critical velocities. This may be explained by the fact that the high-volume fraction of particles having velocity below the critical velocity, which is more than 80%, erodes the surface which in turn reduces the measured deposition efficiency.

Since the addition of $Al_2O_3$ increases the deposition efficiency, the critical velocity decreases accordingly. For example with 30 wt.% of $Al_2O_3$ in the starting powder, the critical velocities for Al, based on the measured deposition efficiency of Al only, are 530 and 660 m/s for the 54NS and the Alfa powders, respectively. The impact of $Al_2O_3$ particles roughen the coating during build-up creating asperities either by forming impact marks or by protruding from the surface. These asperities favor the bonding of incoming Al particles. This aspect will be discussed later. However, this result suggests strongly that the critical velocity depends not only on the materials properties and state (i.e., velocity and temperature) but also on the surface properties and topology.

**Table 1 Velocity of the base powders used in this work**

| Powder | | Velocity, m/s | Standard deviation, m/s |
|---|---|---|---|
| Al | Alfa-Aesar | 584 | 88 |
| Al | Sulzer 54NS | 448 | 80 |
| $Al_2O_3$ | Plasmatec | 580 | 84 |

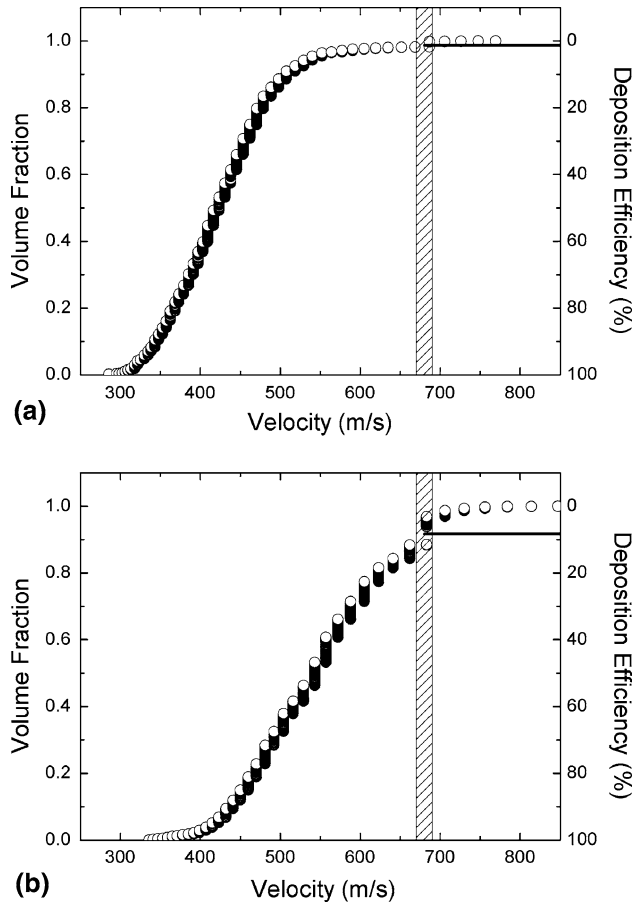


**Fig. 5** Cumulative volume fraction against velocity for (a) the large Al powder (54NS) and (b) the small Al powder (Alfa)

### 3.5 Coating Properties

The hardness of both coating types increases as a function of the $Al_2O_3$ mass fraction entrapped in the coating as shown in Fig. 6. However, the coatings made from the large Al powder are systematically harder than those produced using the small Al powder. This difference in hardness cannot be interpreted by a difference in the hardness of the starting material, the hardness of the large and small powders being 25 and 26 $HV_{10}$, respectively. This difference can be understood by the large size difference of the two Al powders. Indeed, the average mass and velocity ratio of the large to small powder mean particles are about 12 and 0.77, respectively. Consequently, the kinetic energy of the mean large Al powder particles is seven times higher than the one of the mean small Al powder particles. This extra energy in the large

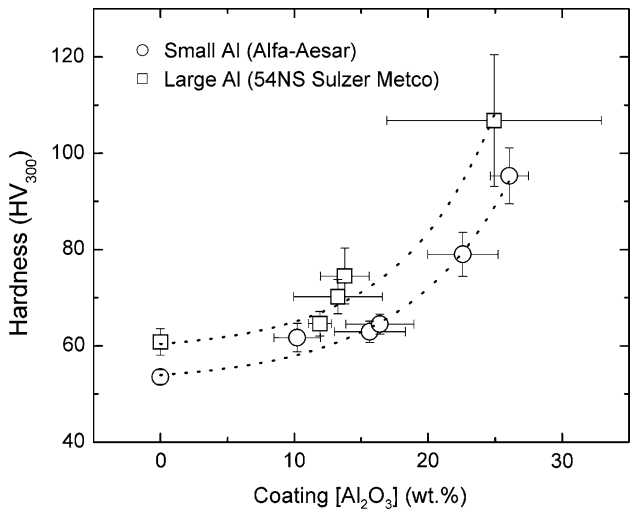


**Fig. 6** Vickers hardness measurements against $Al_2O_3$ concentration into the coating

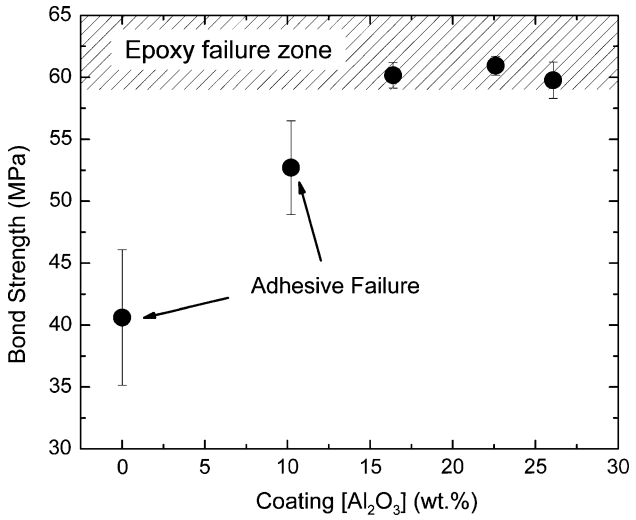


**Fig. 7** Bond strength against coating $Al_2O_3$ concentration

Al powder generates more cold deformation and therefore more strain hardening during deposition. It is worth noting that hardness measurements were made on coatings produced on previously grit blasted mild steel substrates. Using this surface preparation, all coatings were dense, with measured porosity values of less than 2%, contrary to what was obtained for the pure large Al powder coating on polished Al7075 substrate. Despite its higher porosity, the large Al powder coating has denser zones formed from heavily deformed particles that are probably strain hardened.

The results of the adhesion and abrasion tests are presented in Fig. 7 and Table 2, respectively. Considering the rather small differences in hardness and porosity between coatings produced with the small and the large Al powders and because the deposition efficiency is significantly higher with the small Al powder, these experiments were carried out only with the small Al powder mixtures deposited on sandblasted mild steel substrates. The addition of $Al_2O_3$ into the starting Al powder has a beneficial effect on the bond strength. The bond strength was equal to 40 and 53 MPa for pure Al coating and for coating produced with a starting powder having 10 wt.% of $Al_2O_3$, respectively. The failure mode was adhesive for those samples. On the other hand, for samples prepared with powders having 30 wt.% $Al_2O_3$ or more, because the failure mode was in the epoxy glue, the bond strength value is unknown but exceeds 60 MPa. Figure 8 shows SEM back-scattered micrographs of samples produced with different $Al_2O_3$ content in the starting powder. It can be seen that the addition of $Al_2O_3$ particles increases the roughness of the substrate. Indeed, in addition to the grit blasting surface preparation procedure, the incoming cold-sprayed $Al_2O_3$ particles erode the substrate which in turn creates more asperities, mostly micro-asperities, on the substrate surface. In fact, higher is the $Al_2O_3$ content, the higher is the micro-roughness. The incoming Al particles that impale on these asperities are heavily deformed resulting in a strong bonding. Also, higher is the substrate roughening, larger is the contact area between the substrate and the coating thus, higher is the bond strength. Consequently, increasing the $Al_2O_3$ content in the starting Al powder increases the adhesion of the coating on the substrate.

**Table 2 Bond strength test values with failure mode and, volume lost during an abrasion test at 45 N load for 10 min for several small Al (Alfa)-$Al_2O_3$ concentrations**

| Powder [$Al_2O_3$], wt.% | Coating [$Al_2O_3$], wt.% | Bond strength, MPa | Failure mode | Abrasion: volume lost, $mm^3$ |
|---|---|---|---|---|
| 0 | 0 | 40 ± 5 | Adhesive | 17.0 ± 0.7 |
| 10 | 10.2 | 53 ± 4 | Adhesive | 19.8 ± 0.1 |
| 30 | 16.4 | 60 ± 1 | 60% epoxy | 18.2 ± 0.5 |
| 50 | 22.6 | 61 ± 1 | Epoxy | 19.8 ± 0.1 |
| 75 | 26.1 | 60 ± 1 | Epoxy | 18.5 ± 0.6 |

The volume lost during the abrasion tests is nearly constant while the coating hardness increases by a factor two with the $Al_2O_3$ mass fraction increasing from 0 to 26%. This result suggests that the cohesion between the ceramic and ductile particles is poor. The $Al_2O_3$ particles are entrapped during the coating build-up without forming a strong bond with the surrounding Al matrix. This weak cohesion affects the hardness values (Fig. 6) since it involves mostly compressive deformation; however, it does not affect the abrasion resistance (Table 2) since it involves a ''plowing deformation'' of the abrasive particles against the coating surface.

Photographs of the sample surfaces before and after both alternated immersion and salt spray tests are presented in Fig. 9. After the corrosion tests, the accumulated salt on the sample surfaces was removed with a toothbrush and water. The tests were carried out for 1000 h except for the bare substrates whose test duration was reduced to 24 h due to the rapid deterioration of the samples. After the corrosion test, the bare substrates turned red and their surface were severely attacked in only few hours while the coated sample surfaces have whitened out. For the salt spray test, there is no significant difference between coatings having different ceramic content ratio. No surface roughening was observed during that test. On the contrary, for alternated immersion test in saltwater, the surfaces have been roughened and the degree of roughening was found to be a function of the alumina concentration in the coating.

The back-scattered electron micrographs in Fig. 10 show the coating cross section microstructure of a sample produced with 75 wt.% $Al_2O_3$ in the starting powder after alternated immersion test. At low magnitude (Fig. 7b), it can be noted that no localized corrosion occurred on the substrate at the coating-substrate interface in spite of the presence of the $Al_2O_3$ content. On surface, a thin corrosion product film of less than 25 μm can be seen on Fig. 10b. This film gave the coating surface a white color aspect. No corrosion sites can be found at the interface for all conditions studied as seen on Fig. 10a. The cross section micrographs of all coatings showed that the inclusion of ceramic particles into the Al matrix has no detrimental

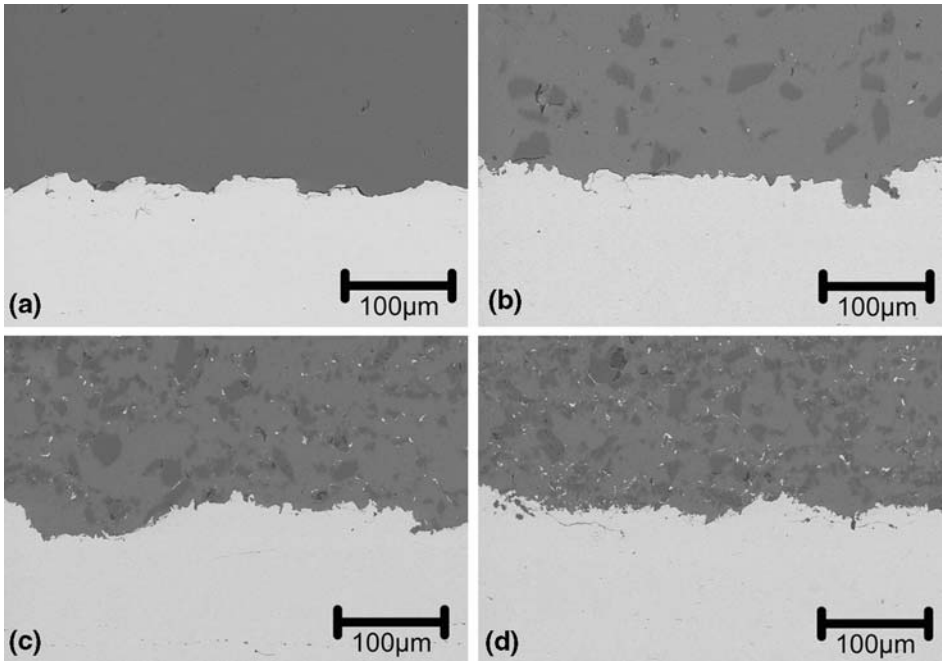


**Fig. 8** Back-scattered electron micrographs of coating cross sections for different $Al_2O_3$ content in the starting powder: (a) 0 wt.%, (b) 10 wt.%, (c) 50 wt.%, and (d) 75 wt.%

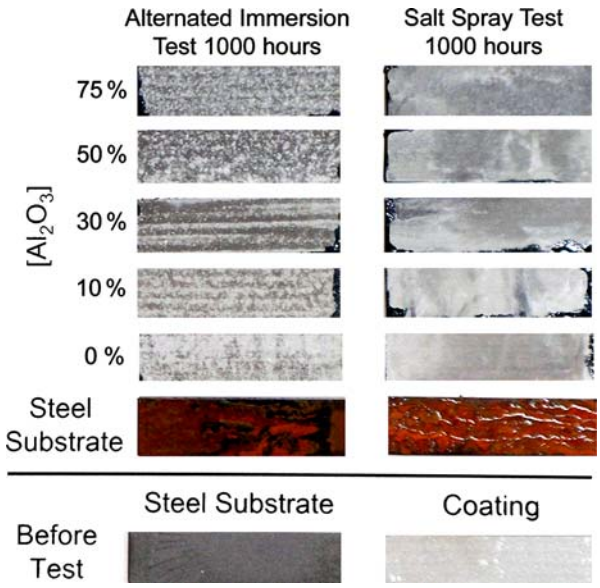


**Fig. 9** Photographs of the Al-$Al_2O_3$ sample surface before and after corrosion tests as a function of the starting powder $Al_2O_3$ ratio. Bare substrates were tested for 24 h

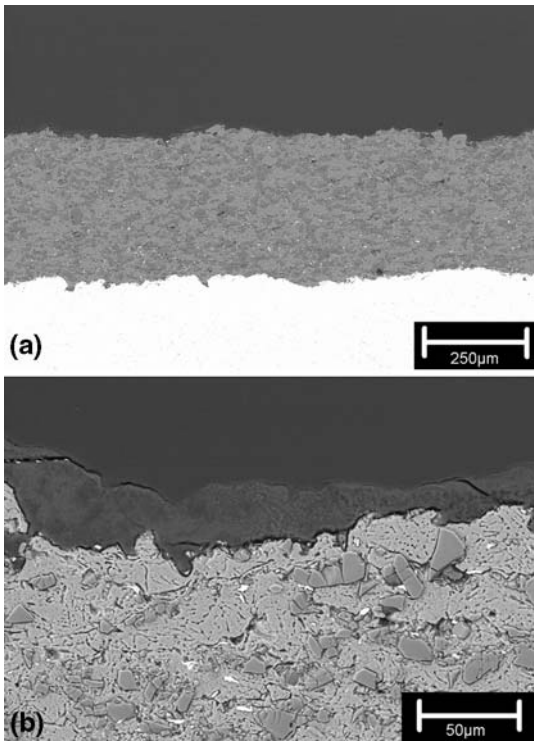


**Fig. 10** Back-scattered electron micrographs of the Al-$Al_2O_3$ coating cross sections after the alternated immersion test for two different magnifications. The starting powder alumina fraction was 75 wt.%

effect on corrosion protection against neither alternated immersion in saltwater nor salt spray environment.

## 4. Conclusion

In this work, we investigated the influence of the Al particle size and $Al_2O_3$ mass fraction in Al-$Al_2O_3$ powder mixtures on the coating deposition and properties. Because the mean velocity of the particles is a function of the particle size, the Al powder having the larger particle size

distribution has a volume fraction of particle having a velocity higher than the critical velocity significantly less than that of the smaller particle Al powder. Its deposition efficiency is consequently lower. However, coatings with the starting powder based on the larger Al particles are systematically harder than coatings made with the smaller size Al powder mixtures. This is likely due to the larger peening effect of the large particles due to their higher kinetic energy. The addition of $Al_2O_3$ to the Al powders helps improving the coating deposition. Optimal deposition efficiency was found for a mass fraction of about 30% of $Al_2O_3$ in the starting powder. Abrasion resistance was found to be independent of the alumina mass fraction in the coatings. Because $Al_2O_3$ particles alone cannot form a coating in our experimental conditions, they play only a role of peening and roughening of the layers during deposition. However, their inclusion in coatings is observed and was limited to about 25 wt.%. Their presence is due to entrapment during deposition of blended Al and $Al_2O_3$ powders. The bonding between Al and $Al_2O_3$ is therefore believed to be weak and the resulting poor cohesion between the two powder types limits any possible improvement of the abrasion resistance of the composite coatings. Such an improvement is generally observed when adding hard particles in a ductile matrix coating. The addition of $Al_2O_3$ to Al powder increased the adhesion of the coating on the substrate. The hard ceramic particles create micro-asperities that favor the bonding of the incoming Al particles and also increase the surface area between the coating and the substrate. The adhesion was higher than 60 MPa for sample produced with more than 30 wt.% $Al_2O_3$. The Al-$Al_2O_3$ coatings proved to be as efficient as pure Al coatings in providing a corrosion protection against alternated immersion in saltwater and against salt spray environment. The inclusion of alumina particles in the aluminum coatings had no detrimental effect on the corrosion protection of the substrate.

## Acknowledgment

The authors acknowledge the technical assistance of J.-F. Alarie, F. Belval, B. Harvey, M. Lamontagne and M. Thibodeau.

## References

1. S.H. Thurston, Method of Impacting One Metal Upon Another, U.S. Patent 705,701, August 12, 1902
2. C.F. Rocheville, Device for Treating the Surface of a Workpiece, U.S. Patent 3,100,724, August 13, 1963
3. A.P. Alkhimov, V.F. Kosarev, and A.N. Papyrin, A Method of 'Cold' Gas-Dynamic Deposition, *Sov. Phys. Doklady*, 1990, **35**(12), p 1047-1049
4. A. Shkodkin, A. Kashirin, O. Klyuev, and T. Buzdygar, Metal Particle Deposition Stimulation by Surface Abrasive Treatment in Gas Dynamic Spraying, *J. Therm. Spray Technol.*, 2006, **15**(3), p 382-386
5. A.I. Kashirin, O.F. Klyuev, and T.V. Buzdygar, Apparatus for Gas-Dynamic Coating, U.S. Patent 6,402,050, June 11, 2002
6. A.P. Alkhimov, A.N. Papyrin, V.F. Kosarev, N.I. Nesterovich, and M.M. Shushpanov, Gas-Dynamic Spraying Method for Applying a Coating, U.S. Patent 5,302,414, April 12, 1994
7. R.G. Maev and V. Leshchynsky, Air Gas Dynamic Spraying of Powder Mixtures: Theory and Application, *J. Therm. Spray Technol.*, 2006, **15**(2), p 198-205
8. R.G. Maev and V. Leshchinsky, Low Pressure Gas Dynamic Spray: Shear Localization During Particle Shock Consolidation, *Building on 100 Years of Success: Proceedings of the 2006 International Thermal Spray Conference*, B.R. Marple, M.M. Hyland, Y.C. Lau, R.S. Lima, and J. Voyer, Eds., May 15-18, 2006 (Seattle, WA, USA), ASM International, 2006
9. E. Irissou and B. Arsenault, Corrosion Study of Cold Sprayed Aluminum Coatings onto Al 7075 Alloy Substrates, *Global Coating Solutions: Proceedings of the 2007 International Thermal Spray Conference*, B.R. Marple, M.H. Hyland, Y.-C. Lau, C.-J. Li, R.S. Lima, and G. Montavon, Eds., May 14-16, 2007, (Beijing, China), ASM International, 2007, p 549-554
10. Z.B. Zhao, B.A. Gillispie, and J.R. Smith, Coating Deposition by the Kinetic Spray Process, *Surf. Coat. Technol.*, 2006, **200**(16-17), p 4746-4754
11. H. Assadi, F. Gartner, T. Stoltenhoff, and H. Kreye, Bonding Mechanism in Cold Gas Spraying, *Acta Mater.*, 2003, **51**(15), p 4379-4394
12. R.C. Dykhuizen and M.F. Smith, Gas Dynamic Principles of Cold Spray, *J. Therm. Spray Technol.*, 1998, **7**(2), p 205-212
13. T. Schmidt, F. Gartner, H. Assadi, and H. Kreye, Development of a Generalized Parameter Window for Cold Spray Deposition, *Acta Mater.*, 2006, **54**(3), p 729-742